ELSEVIER

PHYSICS CONTRIBUTION

DEVELOPMENT OF A MICRO-COMPUTED TOMOGRAPHY–BASED IMAGE-GUIDED CONFORMAL RADIOTHERAPY SYSTEM FOR SMALL ANIMALS

Hu Zhou, Ph.D.,* Manuel Rodriguez, Ph.D.,* Fred van den Haak, A.A.,* Geoffrey Nelson, B.S.,*
Rahil Jogani, M.S.,* Jiali Xu, B.S.,† Xinzhi Zhu, Ph.D.,† Yongjiang Xian, B.S.,§
Phuoc T. Tran, M.D., Ph.D.,* Dean W. Felsher, M.D., Ph.D.,‡ Paul J. Keall, Ph.D.,*
and Edward E. Graves, Ph.D.*

Departments of *Radiation Oncology and ‡Medicine, Molecular Imaging Program at Stanford, Stanford University, Stanford, CA;
†PheniCo, Inc., Fremont, CA; and §Bright Star Machine, Fremont, CA

Purpose: To report on the physical aspects of a system in which radiotherapy functionality was added to a micro-computed tomography (microCT) scanner, to evaluate the accuracy of this instrument, and to and demonstrate the application of this technology for irradiating tumors growing within the lungs of mice.

Methods and Materials: A GE eXplore RS120 microCT scanner was modified by the addition of a two-dimensional subject translation stage and a variable aperture collimator. Quality assurance protocols for these devices, including measurement of translation stage positioning accuracy, collimator aperture accuracy, and collimator alignment with the X-ray beam, were devised. Use of this system for image-guided radiotherapy was assessed by irradiation of a solid water phantom as well as of two mice bearing spontaneous MYC-induced lung tumors. Radiation damage was assessed *ex vivo* by immunohistochemical detection of γH2AX foci.

Results: The positioning error of the translation stage was found to be <0.05 mm, whereas after alignment of the collimator with the X-ray axis through adjustment of its displacement and rotation, the collimator aperture error was <0.1 mm measured at isocenter. Computed tomography image-guided treatment of a solid water phantom demonstrated target localization accuracy to within 0.1 mm. Gamma-H2AX foci were detected within irradiated lung tumors in mice, with contralateral lung tissue displaying background staining.

Conclusions: Addition of radiotherapy functionality to a microCT scanner is an effective means of introducing image-guided radiation treatments into the preclinical setting. This approach has been shown to facilitate small-animal conformal radiotherapy while leveraging existing technology.   © 2010 Elsevier Inc.

Mouse models, Radiotherapy, Image guidance, MicroCT.

INTRODUCTION

Clinical radiotherapy (RT) technology has advanced tremendously since the introduction of the linear accelerator. Advances such as rotating radiation sources, conformal collimators, and image guidance and verification are now commonplace among modern RT equipment. However, analogous systems for the treatment of laboratory animals lack many of these now-standard clinical features. Delivery of radiation treatments to experimental animal models of disease has typically been achieved using fixed radiation sources applying a single radiation field. Sparing of normal tissues is accomplished with radiation shields, commonly sheets of lead or custom-manufactured jigs, bearing openings through which the desired radiation target within the animal is exposed (1–5). The spatial and dosimetric accuracies achievable with these systems are clearly limited and lag significantly behind their clinical counterparts. Except in the case of superficial targets, precise localization of the radiation target as well as sparing of normal tissues are usually not possible with this simple approach.

Recently several three-dimensional (3D) conformal animal RT systems have been developed in an effort to bridge the gap between preclinical and clinical RT technology. Stojadinovic *et al*. (6) have constructed a RT system around a clinical ^{192}Ir high-dose-rate brachytherapy source, delivering beams restricted by fixed collimators from multiple angles to irradiate animals similar to what is achieved with conformal RT. Other groups have built systems from scratch, using X-ray tubes for application of diagnostic and therapeutic radiation. Wong *et al*. (7) have built a stand-alone system encompassing a 225-kVp industrial X-ray tube and individually rotating X-ray, detector, and subject enclosures that can

---

be used to deliver noncoplanar radiation beams to animals. Our group has addressed this technical challenge by adding RT functionality to a micro-computed tomography (microCT) scanner, to leverage existing technology to produce a preclinical system for image-guided RT (8). In this article we report on the physical aspects of this system as well as evaluation of the accuracy of this instrument. In addition, we demonstrate the application of this technology for irradiating tumors growing within the lungs of mice.

METHODS AND MATERIALS

System

GE RS120 MicroCT. An eXplore RS120 microCT scanner (GE Medical Systems, London, ON, Canada) served as the platform for the development of a radiation delivery system. This system can operate at tube currents of 70–120 kVp and has been previously demonstrated to be capable of dose rates of up to 2 Gy per minute beam time at depths relevant to small-animal treatments (9). Figure 1a shows the scanner gantry. The CT isocenter is located at the center of a plexiglass tube (the CT bore). The X-ray tube

and detector are fixed on the gantry on opposite sides of the bore. The RS120 microCT system has a stage housing, inside which an animal couch stage moves along the CT axial direction (the z-axis in the CT coordinate system) to carry the animal into and out of the bore for imaging. A nose cone on this bed allows continuous delivery of isoflurane anesthesia to a subject while it is on the scanner bed.

To serve as a RT device, this system requires several additional functionalities that are not necessary for microCT imaging. These added capabilities include the ability to restrict the width of the beam to target a specific volume of tissue and the ability to shift an arbitrary 3D point within a subject to the system isocenter for treatment. To meet these needs, we integrated a two-dimensional (2D) translation stage with the existing z-stage inside the shield to accomplish 3D movement and mounted a variable-aperture collimator between the source and the bore on the crossbar shown in Fig. 1d.

Animal couch. The microCT includes an animal couch clamped on a motor-driven stage that moves the animal in and out of the scanner along the z-direction, installed inside the X-ray shielded stage housing. We added a 2D stage that moves in the two other directions (x or left/right, and y or up/down) inside the housing, as shown in Fig. 1b. To move the stage within the 10.2-cm bore,
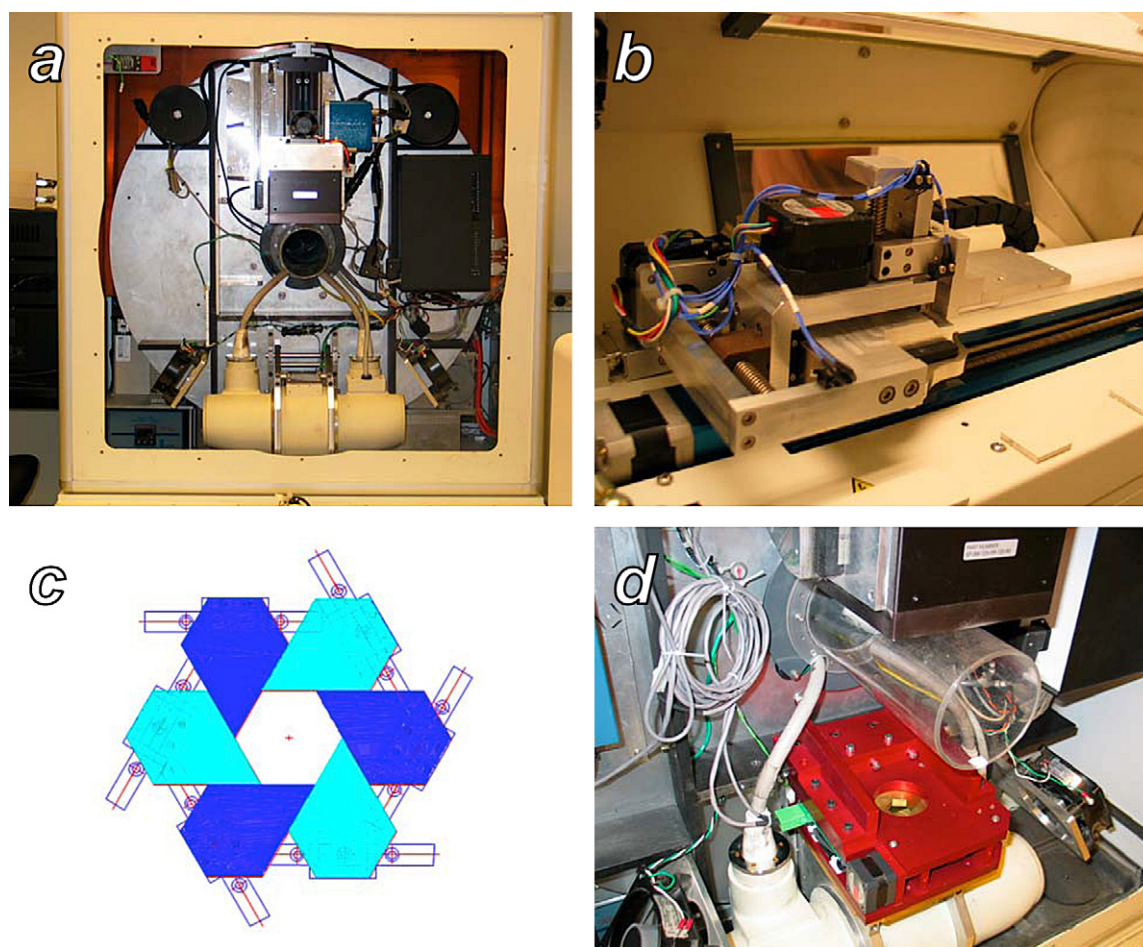

Fig. 1. The GE RS120 microCT and the additional components necessary for small-animal radiotherapy. (a) View of the scanner gantry after removing the X-ray shield and animal stage housing. The large silver disk is the rotating gantry, with the X-ray tube, H-shaped collimator mounting bar, subject bore, and detector arranged bottom to top, respectively. (b) Custom two-dimensional translation stage for subject positioning, mounted on top of the existing z-axis translation stage of the scanner. (c) Schematic representation of a single stage of the variable-aperture collimator, formed by six sliding blocks mounted on linear tracks. (d) Final two-stage collimator apparatus after installation on the H mounting bar of the scanner gantry.

the maximum travel distance in x and y were designed to be 50.8 mm and 20 mm, respectively. The 2D stage is installed on the existing z-stage mount by opening and closing a clamp and can be moved either manually through a control box or through software controls installed on the microCT control PC.

Collimator. A variable-aperture collimator permanently installed on the scanner gantry between the X-ray source and the subject bore allows shaping of the X-ray beam for RT, or alternately passage of the full beam to facilitate imaging without removing the device. The design goal of the collimator was to vary the X-ray beam diameter from 0 (fully closed) to 102 mm (fully open) at the CT isocenter. The attenuation in the shielded area was designed to be more than 95%. The complete collimator assembly and its placement on the scanner gantry are shown in Fig. 1d.

Figure 1c shows the principle of the collimator, in which 12 pentagonal lead-brass blocks were arranged in two planes, forming two stages of collimation. The two stages consist of arrays of sliding brass blocks, which may be adjusted to form a hexagonal aperture as described previously (8). The two hexagonal apertures are arranged coaxially, offset by 30°, and each is driven by a linear stepper motor through a lead screw, a more robust driving mechanism than the rotational scheme described previously. The two stages will hereafter be referred to as the ''near'' (closest to the X-ray source) and ''far'' collimators. By setting the size of the two apertures to a constant ratio, equal to the distance ratio of the two hexagons from the X-ray source spot, a regular dodecagon beam profile is formed. A position sensor attached to each stage reports the aperture size of the stage. A brass plate with a circular opening, attached to near side of the collimator, shields the control electronics within the device from irradiation. A graphical user interface (GUI) on the microCT control personal computer allows the user to specify collimator apertures, either independently or synchronized, to fit the divergence of the X-ray beam.

Treatment planning system. A treatment planning system is under development. This system includes a GUI based on the RT_Image software package (10) and is linked to a Monte Carlo dose computation system based on the EGSnrc code. The GUI allows the user to manually specify a sequence of beams, setting the isocenters, widths, angular directions, and exposure times for each.

Calibration

Translation stage. The geometric calibration of the translation stage determined the relationship between the physical positions and the machine units of the stages. In the calibration each stage was set with a series of machine units, and the physical positions were measured after each movement. The stages were repeatedly moved back and forth to determine the effects of any potential mechanical backlash.

Geometric calibration of the collimator. The geometric calibration of the collimator included two major measurements: the physical aperture vs. machine unit calibration, and the collimator–beam axis alignment. The physical aperture/machine control unit calibration was performed to determine the relationship between the physical aperture size and the machine readings. To find the parameters of this relationship, several cylinders with diameters ranging from 6 mm to 36 mm with precisions of 0.025 mm were prepared. For each measurement, one of these cylinders was inserted in the aperture of one fully open collimator stage, and the aperture was then reduced until the cylinder was tightly held. Calipers were used to verify the collimator aperture size after removal of the cylinder, and the position sensor reading at this location was recorded. These readings were then fit to a linear

function of the cylinder diameter to obtain the calibration parameters. The measurement was repeated several times with the aperture setting from fully closed to fully open, and vice versa.

Alignment of collimator axis with X-ray beam. The X-ray beam axis is defined as a straight line passing the source spot center and perpendicular to the CT axis. Alignment of the collimator axis with this line was necessary to ensure that the collimator focuses the radiation beam on the isocenter regardless of aperture size. Misalignment may result from displacement and/or tilting of the collimator axis with respect to the beam axis. Displacement was measured through several methods, including a split-field test (11), imaging of a fixed object through a collimator at angles of 0° and 180°, and by evaluation of the hexagonal profiles produced by each of the two collimator stages (8). A small tilt of the collimator plane creates an effect similar to displacement in the appearance of the hexagonal profiles of the collimator stages. If the displacement is assumed to be zero, the angle of tilting can be derived from the law of sines. A composite alignment procedure therefore consisted of iterative measurement and correction of the displacement and tilting of the collimator until the error fell within a tolerance of 0.1 mm. Several sets of positioning screws were set to allow reproducible translation and angular positioning of the collimator.

Collimator performance. When adjusting the collimator aperture, the control software compares the current sensor reading with the user-specified new aperture size to calculate the required shift. After performing this shift, the software makes this comparison again and iterates this process until the discrepancy between the desired and actual aperture sizes is below a tolerance. The error tolerance of the collimator aperture measured at the CT isocenter was set to 0.1 mm when the aperture is >20 mm, and 0.05 mm for smaller apertures. These error tolerances were chosen in an effort to balance device accuracy with collimator adjustment time. The performance of the collimator was measured by repeatedly setting the collimator with different apertures and recording the aperture size error and the setting time, to evaluate the reliability of the mechanism and the control algorithm.

Phantom irradiation

To establish that this hybrid microCT/RT system could accurately localize an arbitrary target within a subject for irradiation, a phantom was constructed. The phantom consisted of 10 sheets of solid water measuring $6 \times 6 \times 0.3$ cm stacked to form a cube. Within one of the central sheets, a hole of diameter 0.3 cm was drilled at a location of (10 mm, 10 mm) from the upper left corner. A 3-mm-diameter metal sphere was secured in the center of this hole, and sheets of radiochromic film were sandwiched within the solid water stack above and below the sheet bearing the sphere. This phantom was then placed on the microCT subject bed and secured so that the films and solid water sheets were coplanar with the plane of rotation of the scanner gantry. The phantom was imaged using a standard microCT protocol (400 views, 0.9° view increment, 70 kVp, 40 mA, 25 ms exposure per view). The image data were reconstructed at an isotropic resolution of 0.1 mm per pixel and viewed with RT_Image. The location of the metal sphere was identified in the microCT images, and the translation stage offsets needed to shift the sphere to the scanner isocenter were calculated. These offsets were applied, and subsequently the phantom was irradiated with eight 120-kVp, 50-mA beams spaced at 45° increments, using exposure times calculated from beam commissioning data to deliver a total dose of 1 Gy at isocenter (9). The film was then removed, and the dose profile on it was used to assess the accuracy of targeting of the metal sphere.
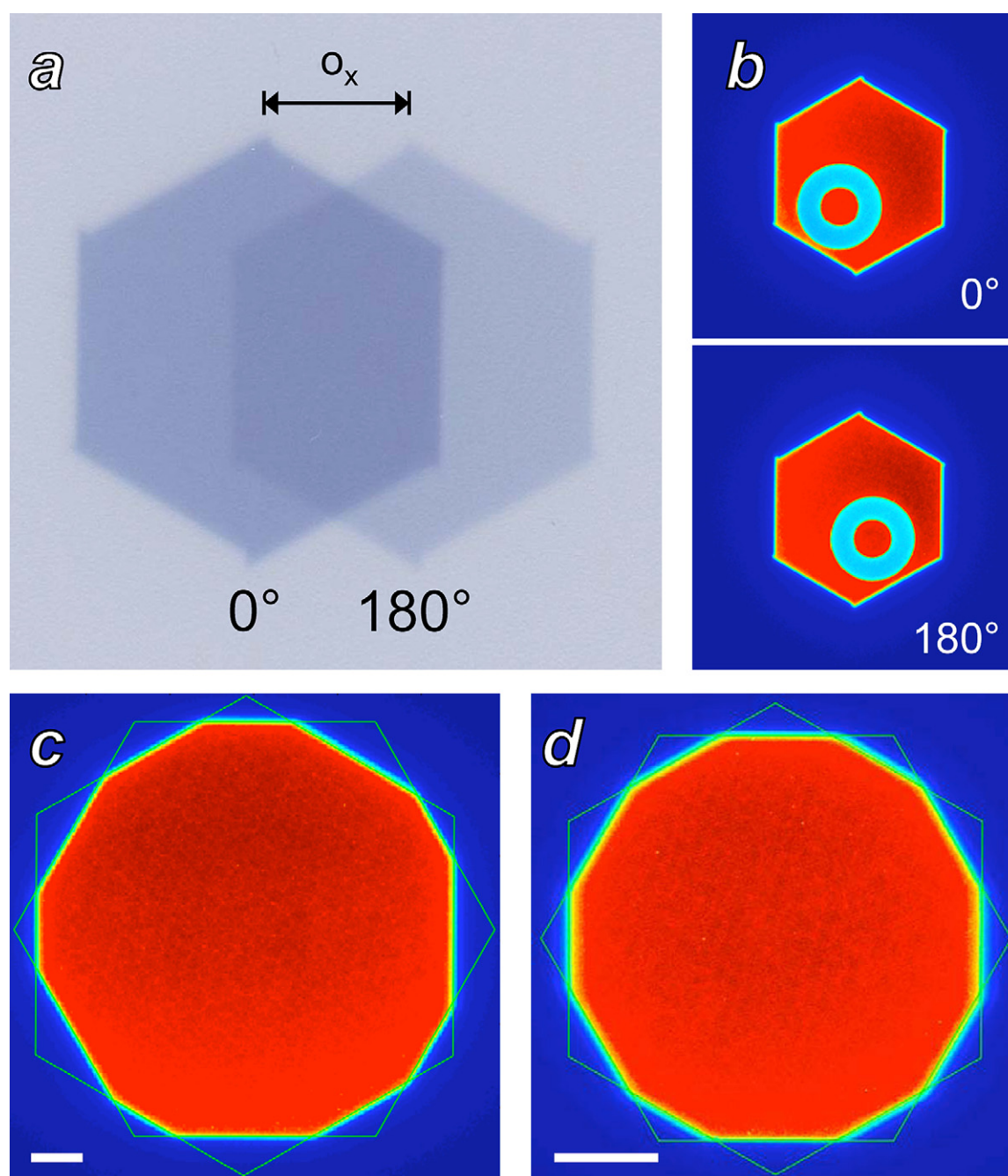
Fig. 2. Measurement of collimator alignment with the X-ray beam axis. (a) Split-field irradiation. The offset o_x between the images from 0° (darker) and 180° (lighter) gantry angles is used to compute the offset of the collimator from the beam axis. (b) Measurement of collimator offset by imaging a fixed object. The average of the object location seen at 0° and at 180° gives the scanner isocenter, whereas the collimator center can be measured according to the hexagonal profile. (c) Measurement of collimator offset by fitting the hexagonal profiles produced by each collimator stage, with both stages set at isocenter apertures of 20 mm. Asymmetry in the dodecagon is apparent, produced by offset between the centers of the two hexagons. The white scale bar is 2.5 mm at isocenter. (d) Two-hexagon analysis after iterative alignment of the collimator with the X-ray beam axis. The collimator apertures are set to 10 mm at isocenter to improve visual detection of any misalignment. The white scale bar is 2.5 mm at isocenter.

Mouse irradiation

To assess whether this unit could be used to deliver conformal RT to a murine subject, we irradiated tumors in the lungs of two mice to a dose of 2 Gy at isocenter. Transgenic mice were created that, when treated with tetracycline, express the MYC oncogene in the cells of the lung. These mice develop spontaneous lung carcinomas within a median of 52 weeks of MYC induction (12). Two such mice

bearing late-stage disease were selected for treatment with RT. A subject mouse was placed on the microCT bed and anesthetized with isoflurane. MicroCT data were acquired as 400 projections equally spaced over 360° (70 kVp, 40 mA, 25 ms exposure per view), which were then reconstructed into volumetric CT images using a cone-beam algorithm. The whole-body dose of the microCT scan was estimated using RT commissioning data to be 6 cGy,

comparable to that reported previously for microCT scanners (13). The reconstructed 3D volume was loaded into RT_Image to localize the tumor and calculate the appropriate position settings for the 3D translation stage and the collimator. After adjusting the stages and collimator, RT was delivered as a series of eight 120-kVp, 50-mA beams equally spaced over 360° to a dose of 2 Gy at isocenter. A Monte Carlo model was used to simulate the dose distribution produced by this treatment (14).

Immediately after irradiation, the mice were killed and tissues harvested. The lungs of the mice including the target tumor were excised, fixed in formalin, and cut into 20-mm sections. They were then stained with antibodies against γH2AX, a histone protein that is recruited to the site of double-strand breaks (15), as well as 4',6-diamidino-2-phenylindole (DAPI) to visualize cell nuclei. These immunohistochemical sections were then visualized with fluorescence microscopy.

RESULTS

System

The custom-designed collimator was successfully installed on the microCT gantry. The weight of the collimator assembly was 17 lb, which was counterweighted on the gantry by the addition of lead disk weights to the outer cylindrical counterweights. MicroCT images acquired before and after installation of the collimator demonstrated no measurable degradation in image quality after addition of the collimator.

Calibration

Translation stage. The motors driving the translation stage in x and y have resolutions of 787.6 and 1400.9 steps/mm, respectively. The reproducibility, determined by comparing the physical position of the device and the motor readings, is better than 0.05 mm in both directions.

Geometric calibration of the collimator. The machine unit/physical aperture relationship was measured by inserting the cylinders of different standard diameters and reading the position sensors of the collimator, from which linear relations were obtained for the near and far stages. The fitting uncertainty was 0.15% on average (maximum 0.36%), obtained from the variation of repeated measurements. The size of these apertures at the isocenter was then measured using both radiochromic film and the CT detector, allowing expression of the relationship between the collimator machine units and the aperture sizes. These relationships were implemented in the collimator control software. As observed previously by Rodriguez *et al.* (9), the penumbras of the near and far colli-

mators were not significantly different, and they were therefore handled identically by the aperture control software.

Alignment of collimator axis with X-ray beam. The collimator alignment procedure required five iterations of the displacement-tilting adjustment and measurement. Figure 2 demonstrates the split-field, imaged object, and two hexagon measurement techniques used to assess displacement. In addition to the displacements required to align the collimator with the beam, a slight tilt was noted that was corrected by elevating the left side of the collimator by 1.4 mm. The displacement and tilting adjustments measured after completion of the alignment procedure were <0.1 mm.

Collimator performance. The results of the performance measurements are listed in Table 1. Aperture sizes at isocenter could be achieved by the control software with errors of <1.0%. Adjustment of the collimator from a fully open position to an aperture relevant for small-animal RT required between 20 and 40 s to iterate to the desired tolerable error.

Phantom irradiation

Figure 3 shows the results of a test designed to evaluate the ability of the system to locate and deliver radiation beams to a target within a subject. A metal sphere served as a CT-visible target within a cubic solid water phantom. Streak and ring artifacts are visible in the reconstructed CT image because of high X-ray attenuation within the sphere. The centroid of the received dose distribution colocalized with the position of the target metal sphere to within ±0.1 mm in the x and y scanner axes. This experiment was repeated with the film positioned in the y and z scanner axes, and similar results were obtained.

Mouse irradiation

Results obtained from irradiation of a tumor-bearing mouse are shown in Fig. 4. Simulation of the dose distribution achieved by a simple eight-field plan using 8-mm beams reveals that the dose to the target achieved the desired level of 2 Gy, whereas doses to surrounding lung were in the range of 0.3 Gy. A star pattern is visible, due to the small numbers of beams used. The total treatment time required for this plan, including setup and delivery, was 45 min. Sections collected from the target tumor immediately after irradiation showed the presence of γH2AX foci, indicating the formation of DNA double-strand breaks. Sections taken from contralateral lung that received a low dose show only background staining.

Table 1. Performance assessment of the collimator apparatus

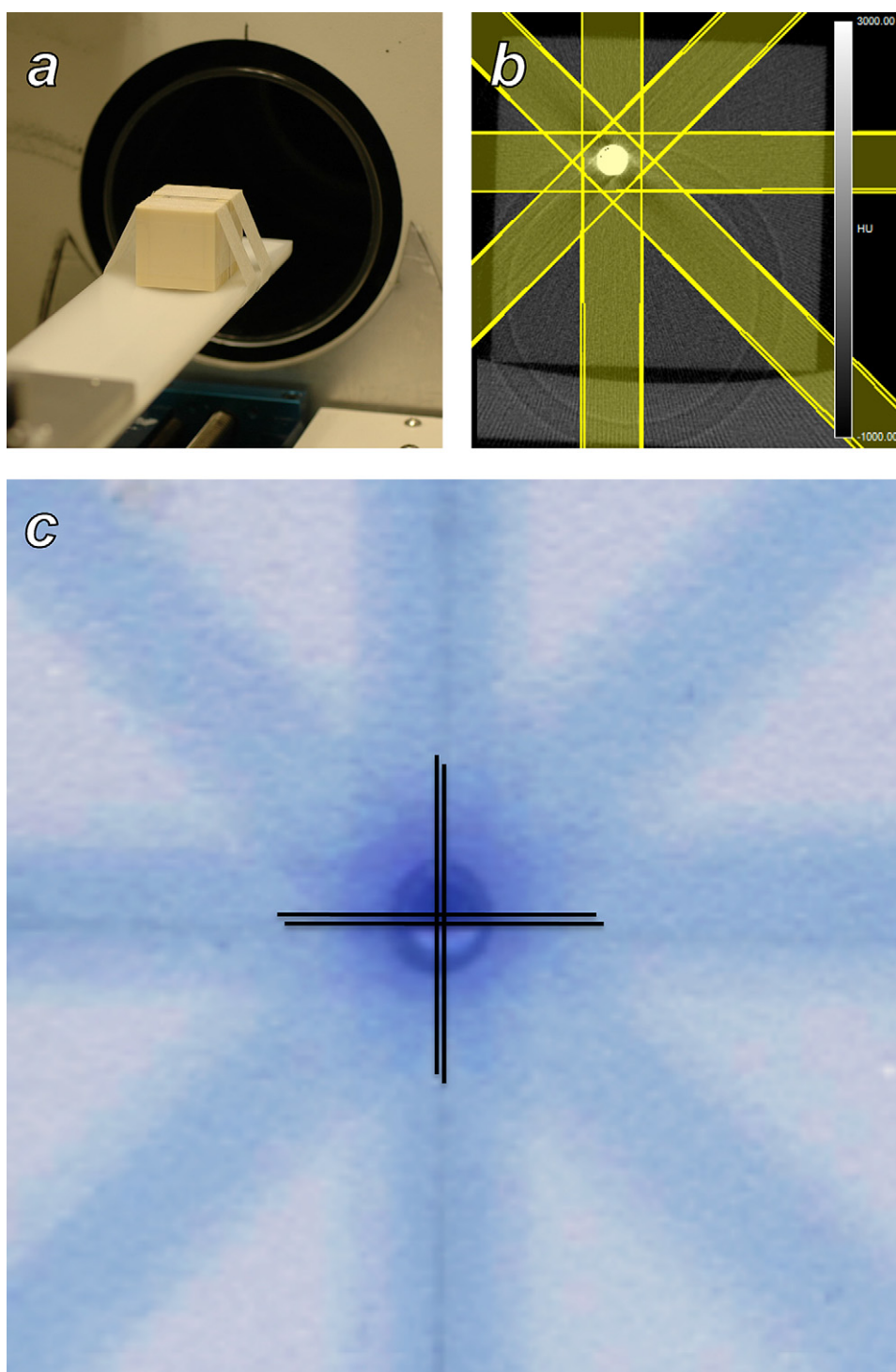| Isocenter aperture (mm)	Near stage			Far stage		
	Error (%)	Closing time (s)	Opening time (s)	Error (%)	Closing time (s)	Opening time (s)
16	0.16	19	23	0.01	16	16
10	0.25	19	24	0.07	19	19
5	0.19	24	24	0.24	19	19
2	0.79	42	26	0.32	24	20

Fig. 3. Evaluation of subject targeting accuracy using a solid water phantom. (a) Phantom containing a metal sphere and radiochromic film was placed on the scanner bed and imaged with microCT. (b) MicroCT image of the phantom showing the metal inclusion, and the radiation treatment plan that was constructed in RT_Image. (c) Superposition of a the solid water/metal sphere phantom and the adjacent irradiated film. Crosshairs identify the positions of the center of the sphere and the center of the delivered dose distribution, which agree to within 0.1 mm.

DISCUSSION

MicroCT presents an intriguing platform for the engineering of small-animal RT devices because of the advanced state of development of this technology. We have added hardware and software to an existing scanner to produce a hybrid imaging and RT system. The 2D translation stage and variable aperture collimator needed to introduce RT capability to this system can be manufactured at a cost of less than $25,000, facilitating commercial development of this system as a low-cost add-on option to existing microCT scanners.
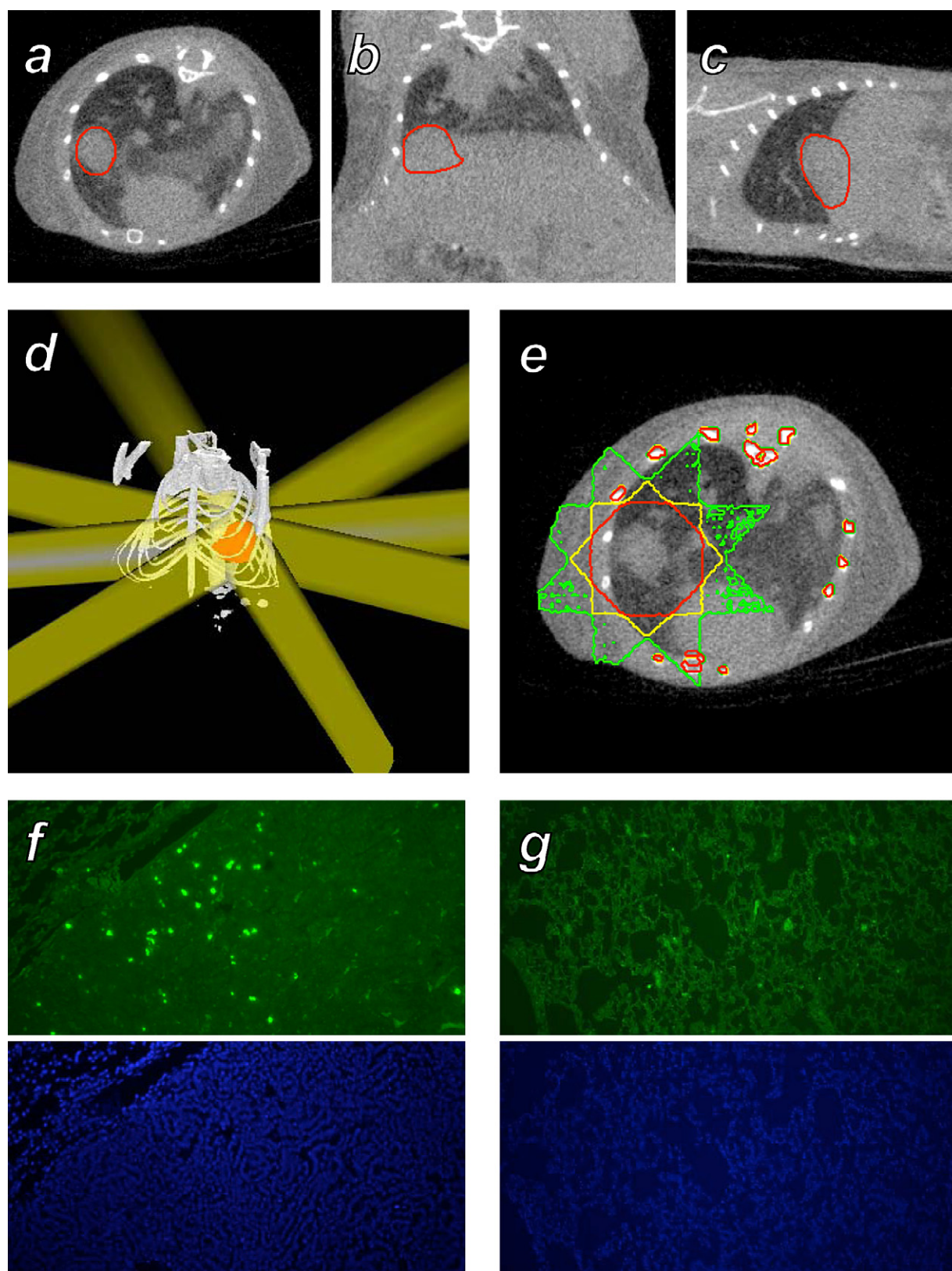
Fig. 4. Treatment of a murine spontaneous lung tumor with the microCT radiotherapy system. (a–c) MYC-induced tumor growing in the base of the right lung of a mouse was imaged with microCT, shown in axial, coronal, and sagittal sections, with the tumor volume outlined in red. (d) Treatment consisting of eight beams of diameter 8 mm at isocenter with angular spacing of 45° was constructed in RT_Image to irradiate the target (red) to a dose of 2 Gy. (e) Monte Carlo simulation of the dose delivered by this plan, with the 1-, 1.4-, and 1.8-Gy isodose contours shown in green, yellow, and red, respectively. (f) Gamma-H2AX (green) and 4',6-diamidino-2-phenylindole (DAPI, blue) immunohistochemical sections from the target tumor. (g) Corresponding immunohistochemical sections from the left lung that received an average dose of 0.3 Gy.

The collimator can be permanently installed on the microCT gantry without compromising imaging ability, and can be removed and reinstalled using positioning markers to quickly achieve alignment with the X-ray axis. Further development of these mechanical components is ongoing, improving their positioning accuracy and mechanical performance while reducing their travel times so as to move toward potential dynamic adjustment of this hardware during radiation treatments. The conformal RT capabilities of this hybrid device were demonstrated in phantoms as well as *in vivo* in a spontaneous murine tumor model. Treatment of rats with this unit is theoretically possible given the beam depth dose profile reported previously (9); however, given the limited travel distances of the motion stages, these larger animals would have to be positioned on the bed such that the desired target was close to the microCT isocenter.

On the basis of the Monte Carlo dosimetry simulation generated for the lung tumor irradiation, it is apparent that the kilovoltage beams of this system deliver significant doses to bony structures. At present it is unknown whether this dose will limit the application of this system. The mass attenuation coefficient of human bone is an order of magnitude greater at the kilovoltage energies of this system relative to the megavoltage energies of clinical RT systems; however, the elemental composition and density of mouse bone have not been rigorously studied. Recent Monte Carlo material modeling efforts have suggested that more rigorous treatment of bony tissues in Monte Carlo simulations is required and suggest that the dose to mouse bones may be overestimated when using material properties derived from human bones (14). Ultimately the problem of bone dose in RT is not unique to this system, because Monte Carlo simulations have demonstrated elevated dose to bone using X-ray energies from 120 to 300 kVp (data not shown). Evaluation of the biologic effects of bone dose in small-animal models will be required to assess the significance of these observations.

The increase in temperature in the X-ray generator and its thermal limits provide constraints on the length of RT treatments and correspondingly the doses that can be delivered. We have measured the temperature rise in the generator during several X-ray delivery sequences and have found that a 6-min X-ray firing (corresponding to a mouse dose of approximately 1 Gy) followed by a 4-min cooling period results in a stable peak generator temperature of 60 °C over repeated firings. The addition of cooling equipment to the generator could compensate for temperature increases to reduce the duration of cooling periods. It is also important to mention that conformal treatment plans using large (more than 10) numbers of beams, in which the dose per beam is <1 Gy, will cause smaller temperature increases for each beam and thus require shorter cooling periods.

Heating of the X-ray tube is a second important consideration. Replacement of the X-ray tube with a more robust model, or alternately use of a larger focal spot at the cost of increased beam penumbra, may be required for RT protocols desiring radiosurgical doses (more than 20 Gy per fraction). Rodriguez *et al.* (9) observed a 0.5-mm penumbra when using the current 0.3-mm focal spot of the X-ray tube. The tube has a second focal spot option of 0.9 mm, which would be expected to increase the observed penumbra to 2 to 3 mm. These two states could be selected on a per-application basis. Scenarios requiring high precision, such as treatment of small (<2 mm) tumors in sensitive sites such as brain or lung could use the small focal spot at the cost of longer treatment times, whereas irradiation of larger targets (large tumors, normal tissues) could reduce treatment times through use of the large focal spot, at the cost of spatial accuracy.

This work has shown that it is technically possible to modify a microCT scanner to serve as a small-animal conformal RT system, operating in a fashion analogous to current clinical image-guided RT devices. Although the spontaneous lung tumor model studied here was treated with only eight beams, in principle this device can deliver large numbers of beams from multiple angles, approaching current arc treatment strategies. We anticipate that the applications of radiation in molecular biology studies of animal tumors using technology such as that demonstrated here will significantly enhance our knowledge of radiobiology and provide a means to study clinically relevant radiation treatment strategies in a preclinical setting.

REFERENCES

1. Knox SJ, Goris ML, Wessels BW. Overview of animal studies comparing radioimmunotherapy with dose equivalent external beam irradiation. *Radiother Oncol* 1992;23: 111–117.

2. Khan MA, Hill RP, Van Dyk J. Partial volume rat lung irradiation: An evaluation of early DNA damage. *Int J Radiat Oncol Biol Phys* 1998;40:467–476.

3. Hillman GG, Maughan RL, Grignon DJ, *et al.* Neutron or photon irradiation for prostate tumors: Enhancement of cytokine therapy in a metastatic tumor model. *Clin Cancer Res* 2001;7: 136–144.

4. Khan MA, Van Dyk J, Yeung IW, *et al.* Partial volume rat lung irradiation: Assessment of early DNA damage in different lung regions and effect of radical scavengers. *Radiother Oncol* 2003; 66:95–102.

5. Hillman GG, Wang Y, Che M, *et al.* Progression of renal cell carcinoma is inhibited by genistein and radiation in an orthotopic model. *BMC Cancer* 2007;7:4.

6. Stojadinovic S, Low D, Hope A, *et al.* MicroRT—small animal conformal irradiator. *Med Phys* 2007;34:4706–4716.

7. Wong J, Armour E, Kazanzides P, *et al.* High-resolution, small animal radiation research platform with x-ray tomographic guidance capabilities. *Int J Radiat Oncol Biol Phys* 2008;71:1591–1599.

8. Graves E, Zhou H, Chatterjee R, *et al.* Design and evaluation of a variable aperture collimator for conformal radiotherapy of small animals using a microCT scanner. *Med Phys* 2007;34: 4359–4367.

9. Rodriguez M, Zhou H, Keall P, et al. Commissioning of a novel microCT/RT system for small animal conformal radiotherapy. *Phys Med Biol*. In press.

10. Graves EE, Quon A, Loo BW. RT_Image: An open-source tool for investigating PET in radiation oncology. *Technol Cancer Res Treat* 2007;6:111–121.

11. Lutz WR, Larsen RD, Bjärngard BE. Beam alignment tests for therapy accelerators. *Int J Radiat Oncol Biol Phys* 1981;7:1727–1731.

12. Tran PT, Fan AC, Bendapudi P, *et al*. Combined inactivation of MYC and K-Ras oncogenes reverses tumorigenesis in lung adenocarcinomas and lymphomas. *PLoS ONE* 2008;3:e2125.

13. Boone JM, Velazquez O, Cherry SR. Small-animal X-ray dose from micro-CT. *Mol Imaging* 2004;3:149–158.

14. Zhou H, Keall PJ, Graves EE. A bone composition model for Monte Carlo x-ray transport simulations. *Med Phys* 2009;36:1008–1018.

15. Rogakou EP, Pilch DR, Orr AH, *et al*. DNA double-stranded breaks induce histone H2AX phosphorylation on serine 139. *J Biol Chem* 1998;273:5858–5868.